

# Density-Functional Theory Molecular Dynamics Simulations and Experimental Characterization of a-Al<sub>2</sub>O<sub>3</sub>/SiGe Interfaces

Evgueni Chagarov,<sup>\*†</sup> Kasra Sardashti,<sup>†</sup> Tobin Kaufman-Osborn,<sup>‡</sup> Shailesh Madisetti,<sup>§</sup> Serge Oktyabrsky,<sup>||</sup> Bhagawan Sahu,<sup>§</sup> and Andrew Kummel<sup>†</sup>

<sup>†</sup>Department of Chemistry and Biochemistry, University of California, San Diego, La Jolla, California 92093, United States

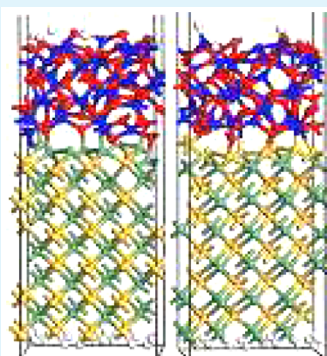
<sup>‡</sup>Applied Materials, Santa Clara, California 95054, United States

<sup>§</sup>GlobalFoundries, Malta, New York 12020, United States

<sup>||</sup>Department of Nanoscale Science and Engineering, University at Albany—State University of New York, Albany, New York 12222, United States

## Supporting Information

**ABSTRACT:** Density-functional theory molecular dynamics simulations were employed to investigate direct interfaces between a-Al<sub>2</sub>O<sub>3</sub> and Si<sub>0.50</sub>Ge<sub>0.50</sub> with Si- and Ge-terminations. The simulated stacks revealed mixed interfacial bonding. While Si–O and Ge–O bonds are unlikely to be problematic, bonding between Al and Si or Ge could result in metallic bond formation; however, the internal bonds of a-Al<sub>2</sub>O<sub>3</sub> are sufficiently strong to allow just weak Al bonding to the SiGe surface thereby preventing formation of metallic-like states but leave dangling bonds. The oxide/SiGe band gaps were unpinned and close to the SiGe bulk band gap. The interfaces had SiGe dangling bonds, but they were sufficiently filled that they did not produce midgap states. Capacitance–voltage (C–V) spectroscopy and angle-resolved X-ray photoelectron spectroscopy experimentally confirmed formation of interfaces with low interface trap density via direct bonding between a-Al<sub>2</sub>O<sub>3</sub> and SiGe.



**KEYWORDS:** SiGe, high-k oxide, oxide-semiconductor interface, DFT, Al<sub>2</sub>O<sub>3</sub>, ab initio, molecular dynamics

## INTRODUCTION

The common problem of many oxide/semiconductor interfaces is a presence of dangling bonds creating midgap or band-edge states and deteriorating electrical properties of the stack. This manuscript demonstrates that, although both Ge- and Si-terminated SiGe surfaces bonded to a-Al<sub>2</sub>O<sub>3</sub> have dangling bonds, they are sufficiently filled so they are electrically passive and can be tolerated. Group IV compound semiconductor oxide interfaces have unique bonding characteristics; since all the semiconductor atoms are isoelectronic, differences in electronic structure at the oxide–semiconductor interfaces between different chemical terminations (for example, Si vs. Ge) are solely due to differences in bond polarization and bond strength instead of simple charge balance (i.e., electron counting rules).

High-k/compound semiconductor group IV structures also have practical importance. For many decades, conventional MOSFET technologies were based on a-SiO<sub>2</sub>/Si interfaces.<sup>1–8</sup> However, as devices were aggressively scaled, use of a-SiO<sub>2</sub> gate oxide became problematic due to shrinking gate oxide thickness causing gate leakage and oxide breakdown.<sup>1,4,5,9,10</sup> This motivated research into high-k gate oxide materials and higher mobility channel materials such as strained Ge or SiGe.<sup>1,5,11–17</sup> Hafnium-based oxides are some of the leading candidates for high-k gate oxides on Si, Ge, or SiGe channels.<sup>13,18–22</sup>

However, there are challenges with incorporation of a-HfO<sub>2</sub> into oxide/channel stacks.<sup>23,24</sup> After depositing a-HfO<sub>2</sub> on SiGe, preferential oxidation of Si near the interface leads to formation of a Ge-rich layer and incorporation of Hf into the interlayer deteriorating oxide electrical properties.<sup>25</sup> Preferential oxidation of Si results in a-SiO<sub>2</sub> formation, which adversely affects equivalent oxide thickness (EOT) scaling.<sup>5,26,27</sup> Ge diffusion into a-HfO<sub>2</sub> can occur creating interface traps and charge traps in the oxide.<sup>28–30</sup> An alternative to a-HfO<sub>2</sub> is a-Al<sub>2</sub>O<sub>3</sub> which has been shown to improve device performance with both Si- and Ge-based channel materials.<sup>31–33</sup> In addition, a-Al<sub>2</sub>O<sub>3</sub> is known to be a good diffusion barrier preventing Ge incorporation into the oxide thus maintaining good oxide properties.<sup>32,34</sup> While a-Al<sub>2</sub>O<sub>3</sub> has an insufficient dielectric constant for high performance MOSFETs, a bilayer of a-HfO<sub>2</sub>/a-Al<sub>2</sub>O<sub>3</sub>/SiGe can be employed so the superior a-Al<sub>2</sub>O<sub>3</sub>/SiGe interface can be utilized.

## RESULTS AND DISCUSSION

This paper presents density-functional theory (DFT) molecular dynamics (MD) simulations which show that a high-quality

**Received:** September 15, 2015

**Accepted:** November 2, 2015

**Published:** November 17, 2015

interface can be formed directly between a-Al<sub>2</sub>O<sub>3</sub> and SiGe with Si- and Ge-terminations without the requirement of an a-SiO<sub>2</sub> or a-GeO<sub>2</sub> interlayer thereby allowing for aggressive EOT scaling. There are many sources of defects at oxide/semiconductor interfaces including intermixing, partially filled dangling bonds (i.e., undercoordinated atoms), metallic bonds, and ionic bonds. The SiGe(001) surface is terminated with dimerized Si and Ge atoms with approximately 1/2 filled dangling bonds. These atoms should be highly reactive, but without charge transfer at the interface, one would expect that any remaining dangling bonds would induce midgap states since they would be half-filled. While Si–O and Ge–O bonds are unlikely to be problematic, bonding between Al and Si or Ge could result in metallic bond formation which usually induces midgap states. As shown below, the internal bonds of a-Al<sub>2</sub>O<sub>3</sub> are sufficiently strong to prevent Al intermixing and to allow just weak bonding to the SiGe surface. These weak interfacial bonds prevent formation of metallic-like states but leave dangling bonds. However, even on the tricoordinated Si and Ge atoms, the dangling bonds are sufficiently filled so midgap state formation is avoided. Furthermore, the Al–Si and Al–Ge bonds are so sufficiently weak that they are nonmetallic.

The Si and Ge terminated surfaces were compared since both can be produced experimentally. Upon annealing in UHV, the SiGe(001) surface spontaneously forms a Ge terminated surface;<sup>35–37</sup> conversely, after bonding to Cl, O, and other strong adsorbates, the SiGe(001) becomes Si terminated after a high temperature anneal.<sup>38,39</sup> The switching from Ge to Si is due to the stronger bonds to oxygen and oxide formed by Si compared to Ge. This allows engineering of Ge vs Si terminated interfaces to the oxide.

High-quality DFT a-Al<sub>2</sub>O<sub>3</sub> samples were generated by separate “melt-and-quench” hybrid classical-DFT MD simulations described in detail elsewhere.<sup>40–42</sup> The amorphous 10–15 samples were generated by varying simulation parameters. To ensure high sample quality, the samples were analyzed to compare properties such as radial distribution function (RDF), angular distribution function (ADF), coordination distribution, average coordination numbers, band gap, etc. to reference experimental and simulated properties. The a-Al<sub>2</sub>O<sub>3</sub> samples including 40 Al and 60 O atoms were generated to match the Si<sub>0.5</sub>Ge<sub>0.5</sub>(001) cross-sectional area to avoid any strain. To increase the variability of the initial interface configurations, the a-Al<sub>2</sub>O<sub>3</sub> bulk sample was cut in two different planes (Cut I and Cut II) forming 2 different oxide initial surfaces in contact with SiGe substrate. Note the exact same cuts were employed for the Ge and Si terminated surfaces. The Si<sub>0.5</sub>Ge<sub>0.5</sub> DFT optimal lattice constant was refined by unit cell relaxation at variable volume. Prior to oxide stacking, two SiGe slabs (2 × 2 × 3 supercells, 48 Si and 48 Ge atoms) were prepared to have Si- and Ge-terminations with (2 × 1) surface reconstruction and relaxed to the ground state. The three bottom SiGe layers were permanently fixed in their bulk-like positions during the full simulation cycle. The bottom SiGe dangling bonds were passivated by relaxed H to simulate bulk continuity. The a-Al<sub>2</sub>O<sub>3</sub> upper surfaces for Cut I and Cut II samples were also passivated by H to restore usual in-bulk coordination of Al and O in a-Al<sub>2</sub>O<sub>3</sub>. All DFT simulations were performed by a VASP plane-wave DFT package using projector augmented-wave (PAW) pseudopotentials (PP), a PBE-GGA exchange-correlation functional for DFT-MD, and a more accurate HSE06 hybrid-functional for final electronic structure calculations.<sup>43–52</sup> The selected validated a-Al<sub>2</sub>O<sub>3</sub> samples (Cut I and

Cut II) were stacked on the SiGe(001) Si- and Ge-terminated (2 × 1) reconstructed surfaces at interfacial bond lengths close to equilibrium values. During the first initial relaxation stage, all SiGe atoms were fixed and the rest of the system (mainly oxide) was partially relaxed for 40 conjugate-gradient (CG) steps to relieve possible interfacial stresses. Afterward, the SiGe atoms were unfixed (except the 3 bottom layers), and the whole stack was annealed at 700 K for 1000 steps with 1 fs timesteps, cooled to 0 K for 200 fs, and relaxed to the ground state below 0.05 eV/Å force tolerance level.

The final relaxed stacks are presented in Figure 1. The analysis of interfacial bonding indicates that for both Ge-terminated interfaces Cut I and Cut II 75% of interfacial bonds are O–Ge and 25% are Al–Ge (Figure 1a,c). For both Si-terminated interfaces Cut I and Cut II, 71% of interfacial bonds are O–Si and 29% are Al–Si (Figure 1b,d). The length of Al–

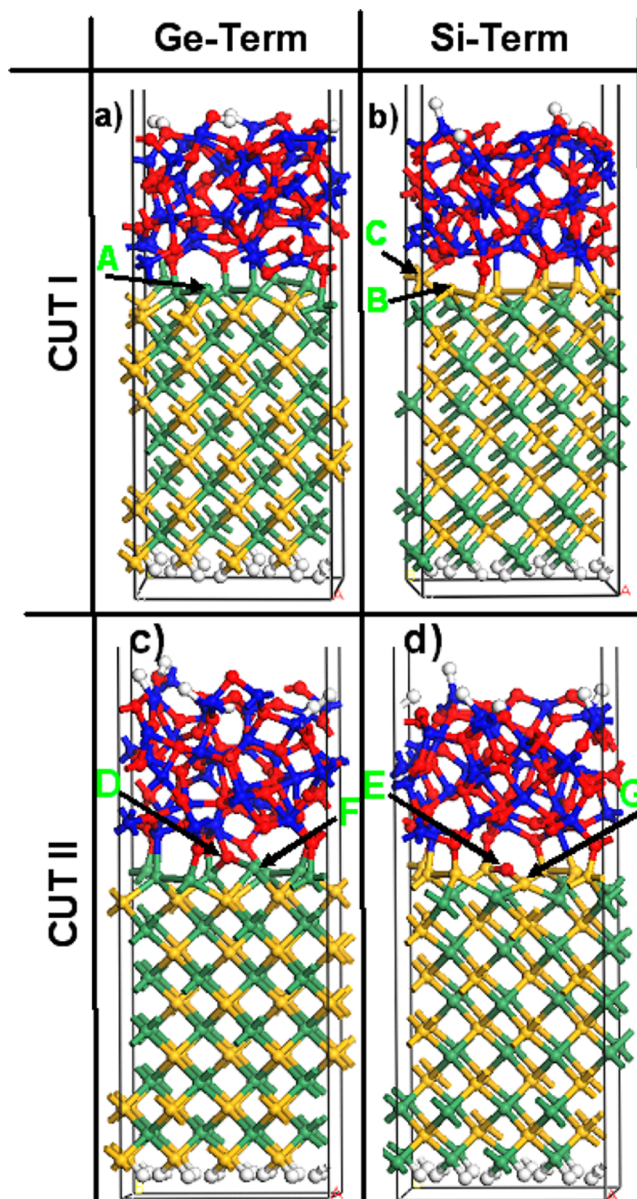


**Figure 1.** a-Al<sub>2</sub>O<sub>3</sub>/Si<sub>0.5</sub>Ge<sub>0.5</sub>(001) DFT-MD annealed and relaxed stacks with oxide Cut I and Cut II: (a, c) Ge-terminated; (b, d) Si-terminated SiGe surfaces. Al, blue; O, red; Si, yellow; Ge, green; H, white.

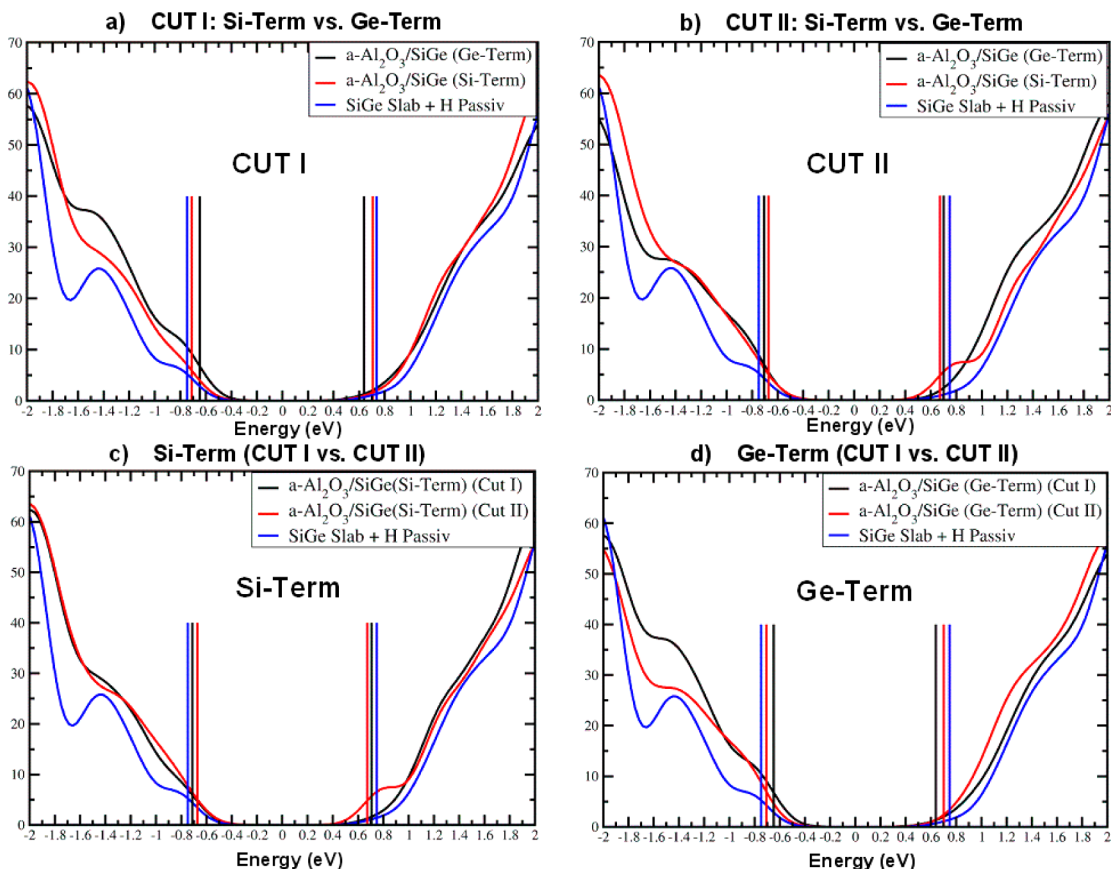


**Figure 2.** Density of states curves, VBM and CBM states for a-Al<sub>2</sub>O<sub>3</sub>/SiGe(Ge-Term), a-Al<sub>2</sub>O<sub>3</sub>/SiGe(Si-Term), and the reference SiGe slab with double H passivation. HSE06 functional. (a) Cut I (Si-Term vs Ge-Term), (b) Cut II (Si-Term vs Ge-Term), (c) Si-Term (Cut I vs Cut II), and (d) Ge-Term (Cut I vs Cut II).

Si bonds is between 2.4 and 2.5 Å with an average length of 2.45 Å. These Al–Si bonds do not produce midgap or band-edge states which will be shown later (Figures 2, 3, and S1). The simulated interfaces with Cut I oxide (Si-Term and Ge-Term) have no Al nor O intermixing and preserve all surface Ge–Ge and Si–Si dimers. For interfaces with Cut II oxide (Si-Term and Ge-Term), 1 oxygen atom intermixes with the SiGe substrates, breaking one Si–Si and Ge–Ge dimer and preserving the other 3 dimers per interface (atoms “D” and “E”, Figure 1). It is likely that the Cut I and II interfaces are different because the oxide cutting procedure produces a more undercoordinated, highly reactive O atom on Cut II. The coordination analysis demonstrates that all surface semiconductor atoms restore 4-fold coordination, forming one additional bond to the oxide, except one 3-fold coordinated Ge for Cut I and II (atom “A” in Figure 1a, atom “F” in Figure 1c), one 3-fold coordinated Si for Cut I and Cut II (atom “B” in Figure 1b, atom “G” in Figure 1d), and one 5-fold coordinated Si atom, forming 2 Si–O bonds to the oxide (atom “C” in Figure 1b). A previous study had examined the interfaces between a-Al<sub>2</sub>O<sub>3</sub> and Ge(001) with DFT-MD annealing at both 700 K and 1100 K.<sup>41,42</sup> It was found that the a-Al<sub>2</sub>O<sub>3</sub>/Ge(001) interface formed only Ge–O bonds and there was substantial breaking of the surface dimer bonds. Several factors contribute to the stability of the a-Al<sub>2</sub>O<sub>3</sub>/SiGe(001) interface compared to a-Al<sub>2</sub>O<sub>3</sub>/Ge(001): (a) Si–Ge back bonds are stronger internal bonds than Ge–Ge, thereby creating a larger activation barrier for oxygen insertion reactions; (b) SiGe has stronger internal

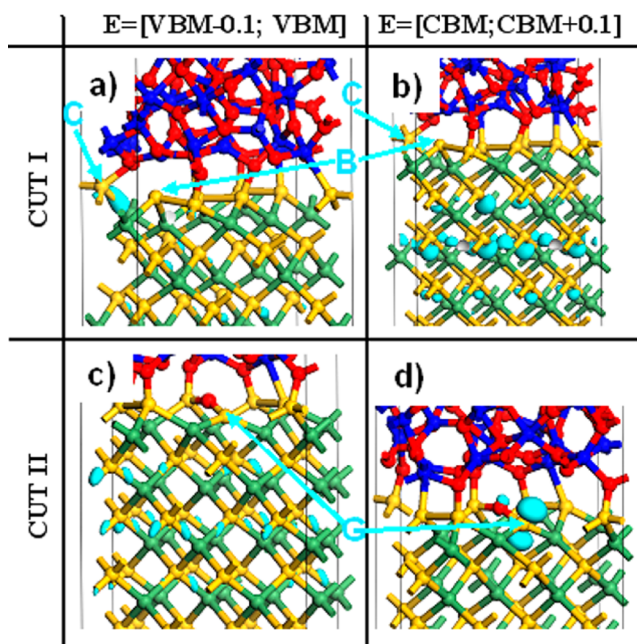


**Figure 3.** Band-decomposed charge density for a-Al<sub>2</sub>O<sub>3</sub>/SiGe(Si-Term) Cut I and Cut II stacks targeting: (a, c) valence band edge states and (b, d) conduction band edge states. HSE06 functional. Al, blue; O, red; Si, yellow; Ge, green.

bonds than Ge, thereby making lattice distortion less thermodynamically favorable.

To obtain a more accurate electronic structure while avoiding band gap underestimation typical for standard DFT, the relaxed stack was rescaled from the PBE to the HSE06 SiGe lattice constant (different by around 1.1%), and the electronic structure with HSE06 hybrid functional was calculated. The high computational cost of HSE06 relaxation of ~200 atom system prevents additional relaxation with HSE06. After rescaling and HSE06 DOS calculation, an absence of significant forces in the oxide was verified.

**Figure 2** presents HSE06 DOS curves for the a-Al<sub>2</sub>O<sub>3</sub>/Si<sub>0.5</sub>Ge<sub>0.5</sub>(001) stacks vs reference Si<sub>0.5</sub>Ge<sub>0</sub> slab with H passivation on the top and bottom surfaces (**Figure S2**). This reference system was chosen since it has the same size as the SiGe portion of the oxide/SiGe stacks and uses the same K-point and Q-point sampling density which makes band gap comparison more rigorous.

Since DOS curves have Gaussian smearing which also smears band gap edges, the valence-band maximum (VBM) and conduction-band minimum (CBM) eigenstates were also added for a more accurate band gap representation. The SiGe reference slab DOS curve was shifted to align deep-level core states with the corresponding peaks of a-Al<sub>2</sub>O<sub>3</sub>/SiGe (Si- and Ge-terminated) stacks. For the oxide/SiGe stacks, the Fermi level is at 0.0 eV (**Figure 2**).

The HSE06 DOS calculations reveal that the a-Al<sub>2</sub>O<sub>3</sub>/SiGe(Si-Term) (Cut I) stack has a band gap of 1.42 eV, which is only 0.06 eV less than the band gap of the reference SiGe slab (1.48 eV); this is not a significant difference (**Figure 2a**). Note that the HSE bandgap of the SiGe reference slab (1.48 eV) is increased vs the experimental bulk value due to quantum confinement caused by the finite cell size. The a-Al<sub>2</sub>O<sub>3</sub>/SiGe(Ge-Term) (Cut I) stack has a slightly narrower band gap of 1.29 eV, which is 0.19 eV less than the SiGe reference slab band gap (**Figure 2a**). Therefore, the a-Al<sub>2</sub>O<sub>3</sub>/SiGe(Si-Term) (Cut I) stack demonstrates a high-quality interface with practically no band gap shrinkage and insignificant band edge states, while the a-Al<sub>2</sub>O<sub>3</sub>/SiGe(Ge-Term) (Cut I) stack has minor band-edge states slightly reducing the band gap. This difference is unexpected since the number of dangling bonds and possibly metallic bonds (Al–Ge and Al–Si) are identical at the two interfaces.

The a-Al<sub>2</sub>O<sub>3</sub>/SiGe (Cut II) (Si-Term) and (Ge-Term) interfaces demonstrate similar bandgaps with no midgap and few minor band-edge states (**Figure 2b**). The a-Al<sub>2</sub>O<sub>3</sub>/SiGe (Si-Term) (Cut II) interface has a bandgap of 1.34 eV, which is 0.14 eV less than the reference SiGe slab bandgap. This bandgap shrinkage is caused mainly by a state near the CB edge and is analyzed in more detail below (**Figure 2b**). The a-Al<sub>2</sub>O<sub>3</sub>/SiGe (Ge-Term) (Cut II) has a bandgap of 1.41 eV, which is only 0.07 eV less than the SiGe reference slab bandgap. The prominent increase in states near the CB for the a-Al<sub>2</sub>O<sub>3</sub>/SiGe (Si-Term) (Cut II) relative to a-Al<sub>2</sub>O<sub>3</sub>/SiGe (Ge-Term) (Cut II) is primarily due to a state beyond the CB edge, and thus, only a small difference (0.07 eV) is observed in the band gap.

To investigate variation between a-Al<sub>2</sub>O<sub>3</sub>/SiGe (Si-Term) Cut I and Cut II interfaces, their DOS curves were compiled on **Figure 2c**. These DOS curves show strong similarity except one defect state near the CB edge for the Cut II interface. The a-Al<sub>2</sub>O<sub>3</sub>/SiGe (Ge-Term) Cut I and Cut II DOS curves were compiled on **Figure 2d** demonstrating strong similarity with very minor deviations near the VBM.

To investigate the source of band-edge states in a-Al<sub>2</sub>O<sub>3</sub>/SiGe(Ge-Term) DOS, band-decomposed charge density calculations were performed for energy intervals [VBM – 0.1 eV, VBM] and [CBM, CBM + 0.1 eV] (**Figures 2–4**). For a-

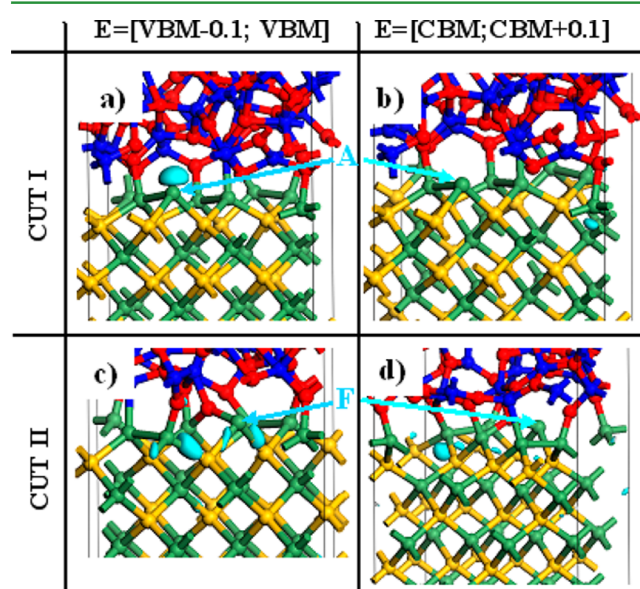


**Figure 4.** Band-decomposed charge density for a-Al<sub>2</sub>O<sub>3</sub>/SiGe(Ge-Term) Cut I and Cut II stacks targeting: (a, c) valence band edge states and (b, d) conduction band edge states. HSE06 functional. Al, blue; O, red; Si, yellow; Ge, green.

Al<sub>2</sub>O<sub>3</sub>/SiGe(Ge-Term) (Cut I) stack, VBM = −0.65 eV and CBM = +0.64 eV with E(Fermi) = 0.0 eV. The 3D visualized states for these intervals are presented in **Figure 4a,b**. The largest band-edge state for Cut I near VBM is localized at the 3-fold under-coordinated Ge atom “A” with a dangling bond and forming no bond to the oxide (**Figure 4a**). The conduction band-edge state for Cut I is much smaller in amplitude and is localized at the 4-fold properly coordinated surface Ge, which has three almost planar strained bonds giving rise to a minor band-edge state near the CBM (**Figure 4b**). Consequently, the main source of band-edge states for the a-Al<sub>2</sub>O<sub>3</sub>/SiGe(Ge-Term) (Cut I) stack is the 3-fold under-coordinated Ge atom “A” with a dangling bond.

For the a-Al<sub>2</sub>O<sub>3</sub>/SiGe (Ge-Term) (Cut II) interface, the bandgap reduction is only 0.07 eV vs SiGe reference slab bandgap. The VBM band-edge state is localized near 3-fold coordinated Ge atom “F” forming no bond to the oxide and another Ge atom forming a strained bond to the O atom (**Figure 4c**). The CBM band-edge state is localized at another Ge atom forming a strained bond to the O atom (**Figure 4d**).

Band-decomposed charge density calculations were performed for the a-Al<sub>2</sub>O<sub>3</sub>/SiGe(Si-Term) Cut I and Cut II stacks visualizing [VBM – 0.1 eV, VBM] and [CBM, CBM + 0.1 eV] energy intervals (**Figure 3**). Since the band gap of the Al<sub>2</sub>O<sub>3</sub>/SiGe(Si-Term) (Cut I) stack is very close to the bulk reference band gap (reduction is only 0.06 eV), these are mainly delocalized states at bulk Si–Ge bonds (**Figure 3b**) and one subsurface strained Si–Ge bond (**Figure 3a**) near the Si atom “C”. In contrast to a-Al<sub>2</sub>O<sub>3</sub>/SiGe(Ge-Term) (Cut I) (**Figure 4a,b**), for both [VBM – 0.1 eV, VBM] and [CBM, CBM + 0.1 eV] intervals of a-Al<sub>2</sub>O<sub>3</sub>/SiGe(Si-Term) (Cut I), the 3-fold coordinated surface Si atom “B” has no band edge states. The a-Al<sub>2</sub>O<sub>3</sub>/SiGe (Si-Term) (Cut II) interface has a weak VBM

band-edge state mainly delocalized at bulk Si–Ge bonds (Figure 3c). The CBM band-edge state for the a-Al<sub>2</sub>O<sub>3</sub>/SiGe (Si-Term) (Cut II) is a more pronounced defect state localized at 3-fold coordinated Si atom “G” (Figure 3d). Although this state is more significant, it penetrates only 0.07 eV into the reference SiGe slab bandgap leading to very minor bandgap reduction.

The valence band edge states from the 3-fold under-coordinated Ge atom at the Al<sub>2</sub>O<sub>3</sub>/SiGe(Ge-Term) (Cut I) interface contrast with the near absence of a band edge state from the under-coordinated Si atom at the a-Al<sub>2</sub>O<sub>3</sub>/SiGe(Si-Term) (Cut I) interface. The difference can be explained by more filled dangling bonds usually being electrically and chemically passive because filled dangling bonds have tightly bound electrons. Conversely, less filled dangling bonds are usually chemically reactive and form band-edge or midgap states because the electrons are weakly bound. To compare dangling bond filling, total charge field was visualized in 3D for all 4 simulated interfaces with the same isolevel of 0.45 (Figure 5). While the 3-fold coordinated Ge (atom “A”) shows no

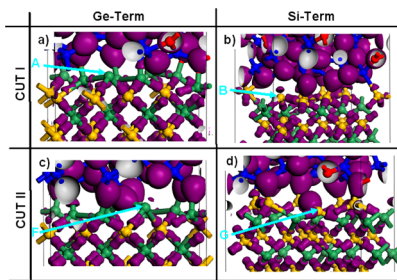


**Figure 5.** Total charge density for a-Al<sub>2</sub>O<sub>3</sub>/Si<sub>0.5</sub>Ge<sub>0.5</sub>(001) stacks with oxide Cut I and Cut II: (a, c) Ge-terminated; (b, d) Si-terminated SiGe surfaces. Al, blue; O, red; Si, yellow; Ge, green.

charge at the dangling bond at this isolevel (Figure 5a), the 3-fold coordinated Si (atom “B”) clearly shows higher charge at the similar dangling bond (Figure 5b). It clearly indicates that the dangling bond at 3-fold Ge atom “A” is less filled (total bandgap reduction of 0.19 eV) than the more filled dangling bond at 3-fold coordinated Si atom “B” (total band gap reduction is only 0.06 eV). The comparison of total charge for Cut II interfaces indicates that 3-fold coordinated Ge (atom “F”) shows charge at the dangling bond (total bandgap reduction is only 0.07 eV), while Si (atom “G”) shows no charge (band gap reduction of 0.14 eV) (Figures 2–5).

To determine the filling of the dangling bonds, Bader charge calculations were performed with core-correction and HSE06 functional to evaluate charge transfer to/from interfacial 3-fold coordinated Ge and Si atoms (Figure 1).<sup>53–55</sup> The SiGe bulk has some Bader charge transfer and bond polarity due to difference in electronegativity. The bulk Ge atoms in the oxide/SiGe stack have an average electron charge of −4.21 lel (for SiGe bulk unit cell Ge electron charge is −4.16 lel) while the bulk Si in the oxide/SiGe stack has an average electron charge of −3.79 lel (for SiGe bulk unit cell Si electron charge is −3.84 lel).

Bonding to the oxide tends to reduce the Bader charge in the surface of Si and Ge since the majority of bonds are to oxygen. The Cut I Si surface atoms bonded to O lose an average of 0.54 lel of electron charge (becoming −3.25 lel) vs in-bulk atoms (−3.79 lel) while similar Cut II Si surface atoms bonded to O lose an average of 0.80 lel of electron charge (becoming −2.99

lel) vs in-bulk atoms. The Cut I Ge surface atoms bonded to O lose an average of 0.46 lel of electron charge (becoming −3.75 lel) vs in-bulk atoms (−4.21 lel), while the Cut II Ge surface atoms bonded to O lose an average of 0.70 lel of electron charge (becoming −3.51 lel) vs in-bulk atoms. In sum, the charge transfer from bonding to the O atoms is very similar for Si and Ge.

Bader charge analysis indicates that the Si atoms forming bonds to Al at Si-terminated Cut I surface have an average of 0.60 lel of greater negative electron charge (becoming −4.39 lel) vs Si in-bulk atoms (−3.79 lel) and Si atoms on the Si-terminated Cut II surface forming bonds to Al have an average of 0.37 lel of greater negative electron charge (becoming −4.16 lel) vs Si in-bulk atoms. The Ge atoms forming bonds to Al at Ge-terminated Cut I surface have an average of 0.34 lel of greater negative electron charge (becoming −4.55 lel) vs in-bulk Ge atoms (−4.21 lel), while Ge atoms on the Ge-terminated Cut II surface forming bonds to Al have an average of 0.28 lel of greater negative electron charge (becoming −4.49 lel) vs in-bulk Ge atoms. In sum, the Si atoms are better charge acceptors from Al than Ge atoms. The Si surface atoms forming bonds to the oxide have larger electron accumulation vs in-bulk values than similar surface Ge atoms making bonds to a-Al<sub>2</sub>O<sub>3</sub>.

For the Cut-I a-Al<sub>2</sub>O<sub>3</sub>/SiGe (Ge-Term) interface, the 3-fold interfacial Ge atom (atom “A”) is more positively charged relative to in-bulk Ge atoms by 0.23 lel (Figure 1a). However, 3-fold interfacial Si (atom “B”) in the Cut-I a-Al<sub>2</sub>O<sub>3</sub>/SiGe (Si-Term) interface is more negatively charged by 0.42 lel relative to in-bulk Si atoms (Figure 1b). This is consistent with the tricoordinated atoms having only two polar Si–Ge bonds.

Comparing absolute values of Bader charges, 3-fold interfacial Ge (atom “A”, Cut I) has an electron charge of −3.98 lel, while 3-fold interfacial Si (atom “B”, Cut I) has an electron charge of −4.21 lel (Figure 1). Therefore, this 3-fold interfacial Si atom “B” is more negative than the 3-fold interfacial Ge atom “A”. The charge values indicate that the interfacial dangling bond of 3-fold Si atom “B” is more filled and more electrically passive than the less filled and more electrically active dangling bond of 3-fold interfacial Ge atom “A” (Figure 1). A possible reason is that Si–Al bonds pull more electron charge to the semiconductor than the Ge–Al bonds while O–Si and O–Ge bonds have roughly equal electron depletion of the semiconductor.

Cut II had a different initial oxide surface than Cut I which created an oxygen transfer at the interface. For the Cut-II a-Al<sub>2</sub>O<sub>3</sub>/SiGe (Ge-Term) interface, the 3-fold coordinated Ge atom “F” exhibits behavior similar to Cut I being more positively charged by 0.63 lel relative to in-bulk Ge atoms since it is bound to the more electronegative O atom breaking the Ge–Ge dimer (Figure 1c). In terms of absolute Bader charges, this 3-fold interfacial Ge atom “F” (Cut II) has an electron charge of −3.58 lel. There is a small VB state on the back-bond of atom “F” consistent with strained bond angles for the undercoordinated 3-fold Ge atom “F” in Cut II (Figure 4c).

The 3-fold interfacial Si (atom “G”) for the a-Al<sub>2</sub>O<sub>3</sub>/SiGe (Si-Term) (Cut II) interface is very different from the 3-fold interfacial Si in Cut I (atom “B”) having a pronounced CBM band-edge state (Figures 1d, 2c, and 3d). However, this Si-created band-edge state penetrates into the SiGe reference bandgap by only 0.07 eV creating a very minor band gap decrease. The Bader charge analysis indicates that this 3-fold Si (atom “G”) has an electron charge of −3.00 lel, which makes it 0.79 lel more positive than the stack in-bulk Si atoms. This is in

contrast to the  $-4.21\text{ eV}$  on the 3-fold interfacial Si atom “B” in Cut I. The Cut II Si atom “G” is more positive than bulk Si atoms because it is bound to more electronegative O atom breaking Si–Si dimer. Since this interfacial Si atom “G” is more positive, it has a less filled and more chemically active dangling bond creating a band-edge state which completely correlates with the 3-fold Ge-atom behavior described above. It is noted that, since this is a less filled dangling bond on Si, it would probably be readily passivated during annealing of the gas to form a Si–H bond, which will produce no states in the band gap.

Experimental results are consistent with an abrupt interface between SiGe and a thin a-Al<sub>2</sub>O<sub>3</sub> layer. Kaufman-Osborn et al. performed XPS studies of trimethyl aluminum and H<sub>2</sub>O<sub>2</sub> dosing of SiGe(001).<sup>56</sup> Prior to annealing, the interface was dominated by Ge<sup>2+</sup> consistent with Ge–O–Al bonds with no GeO<sub>2</sub> or SiO<sub>x</sub>. After annealing, the interface was dominated by Si<sup>2+</sup> consistent with formation of Si–O–Al bonds with no GeO<sub>2</sub> or SiO<sub>x</sub>. Electrically, the annealed interface was unpinned, consistent with the DFT results.

To experimentally determine the correlation between bonding and electronic structure at a-Al<sub>2</sub>O<sub>3</sub>/SiGe interface, metal oxide semiconductor capacitors (MOSCAPs) were fabricated by depositing 3 nm of Al<sub>2</sub>O<sub>3</sub> on SiGe(001), with 30% Ge, via atomic layer deposition (ALD). SiGe(001) samples were cleaned by cyclic HF/H<sub>2</sub>O prior to ALD. Capacitance–voltage measurements were performed on the MOSCAPs at various frequencies ranging from 1 kHz to 1 MHz.

a-Al<sub>2</sub>O<sub>3</sub>/SiGe MOSCAPs were fabricated by depositing 3.0 nm of a-Al<sub>2</sub>O<sub>3</sub> on clean SiGe(001) surfaces. In order to prepare a clean surface for ALD, SiGe(001) samples were cleaned by cyclic HF/H<sub>2</sub>O clean. a-Al<sub>2</sub>O<sub>3</sub> deposition was performed by atomic layer deposition (ALD) at 120 °C where 30 consecutive cycles of 200 ms of trimethylaluminum (TMA) and 50 ms of H<sub>2</sub>O were dosed on the sample surface by pulse valves. After each pulse, a 6 s purge was applied. The chamber base pressure during the ALD process was 1.7 Torr. After oxide deposition, Ni gate metal dots of 150 to 200 μm diameter were deposited on the oxide using thermal evaporation. Fully fabricated MOSCAPs were annealed in forming gas (5% H<sub>2</sub>, 95% N<sub>2</sub>) at 250 °C for 15 min. Capacitance–voltage (C–V) spectroscopy was conducted on the Ni/a-Al<sub>2</sub>O<sub>3</sub>/SiGe MOSCAPs with AC modulation amplitude of 30 mV, in the gate bias range of  $-2$  to  $2\text{ V}$ , at multiple frequencies from 1 kHz to 1 MHz (Figure 6).

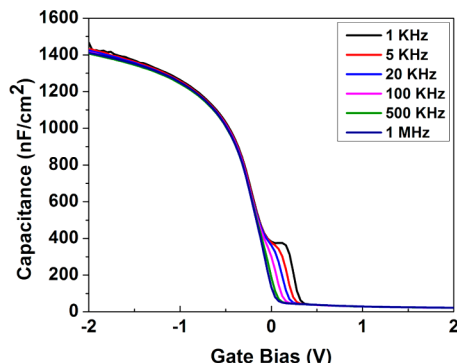


**Figure 6.** Capacitance–voltage curves for a Ni/a-Al<sub>2</sub>O<sub>3</sub>/SiGe(100) MOSCAP at various frequencies from 1 kHz to 1 MHz.

Using the C–V results at 1 kHz and 1 MHz, the density of interface traps ( $D_{it}$ ) was calculated as

$$D_{it} = \frac{1}{q} \left( \frac{C_{OX}C_{LF}}{C_{OX} - C_{LF}} - \frac{C_{OX}C_{HF}}{C_{OX} - C_{HF}} \right)$$

where  $q$  is the electron charge ( $=1.6 \times 10^{-19}\text{C}$ ),  $C_{OX}$  is the oxide capacitance,  $C_{LF}$  is the low frequency capacitance (1 kHz), and  $C_{HF}$  is high frequency capacitance (1 MHz). On the basis of this method, the maximum  $D_{it}$  calculated near the flat band region was estimated as  $3.13 \times 10^{12} \text{ eV}^{-1}\text{cm}^{-2}$ .

Using the high–low CV technique, density of interface traps ( $D_{it}$ ) was estimated as  $3.13 \times 10^{12} \text{ cm}^{-2} \text{ eV}^{-1}$ , which is the lowest ever achieved for high-k oxide/SiGe interfaces and is comparable to Ge MOSCAPs with 1 nm thick interfacial Ge oxynitride layers ( $3 \times 10^{11} \text{ cm}^{-2} \text{ eV}^{-1}$ ).<sup>57</sup> Lower  $D_{it}$  levels ( $<10^{11} \text{ cm}^{-2} \text{ eV}^{-1}$ ) for Ge have only been achieved through formation of GeO<sub>2</sub> interfacial layers between high-k oxides and Ge.<sup>58</sup>

To determine the interfacial composition, angle resolved X-ray photoelectron spectroscopy (AR-XPS) was performed on Al<sub>2</sub>O<sub>3</sub>/SiGe(001) (Figure 7). SiGe samples were cleaned by cyclic HF/H<sub>2</sub>O clean followed by 8 cycles of Al<sub>2</sub>O<sub>3</sub> ALD at 120 °C. Samples were subsequently annealed in forming gas (5% H<sub>2</sub>, 95% N<sub>2</sub>) at 250 °C for 15 min. AR-XPS measurements were obtained by a VG Theta Probe system with an Al K $\alpha$  excitation source (1486.7 eV). AR-XPS spectra were obtained in the takeoff angle range of 26.75° to 79.25° with 7.5° steps. Figure 7 shows the Si 2p and Ge 3d spectra measured at various takeoff angles. The high binding energy shoulders for Si 2p and Ge 3d peaks correspond to SiO<sub>x</sub> and GeO<sub>x</sub>, respectively. This is consistent with formation of no SiO<sub>2</sub> and GeO<sub>2</sub> at the a-Al<sub>2</sub>O<sub>3</sub>/SiGe(001) interface.

Thickness of the interfacial oxide (SiO<sub>x</sub> and GeO<sub>x</sub>) has been estimated with the Beer–Lambert equation in conjunction with oxide/substrate intensity ratio as a function of the takeoff angle. The estimated interfacial oxide thickness is 4 Å which is equivalent to a 1–1.5 monolayer. This 1–1.5 monolayer of interfacial oxide is consistent with formation of Si–O–Al and Ge–O–Al at the interface, the absence of SiO<sub>2</sub> and GeO<sub>2</sub> at the a-Al<sub>2</sub>O<sub>3</sub>/SiGe(001) interface, and direct bonding of the oxide to the surface without interfacial oxide formation. The combination of the C–V measurements and the XPS measurements is consistent with the DFT showing that direct bonding of a-Al<sub>2</sub>O<sub>3</sub> to SiGe(001) can occur without significant interfacial trap state formation.

Recently, there have been several papers on interfaces of gate oxides on SiGe with a focus on GeO<sub>x</sub> at the interface and Ge diffusion into the gate oxide. However, most have focused on HfO<sub>2</sub> and purposeful formation of nitrides<sup>59,60</sup> or SiO<sub>2</sub><sup>61</sup> interlayers to prevent direct bonding of the HfO<sub>2</sub> to the SiGe since Ge readily diffuses into HfO<sub>2</sub>. Conversely, Han et al.<sup>62,63</sup> studied postdeposition plasma nitridation of Al<sub>2</sub>O<sub>3</sub>/Si<sub>0.75</sub>Ge<sub>0.25</sub>(001). Plasma nitridation was compared to plasma oxidation at 300 °C; these plasma processes were performed after 1 nm of Al<sub>2</sub>O<sub>3</sub> ALD and prior to ALD of the remaining 4 nm of oxide; an N<sub>2</sub> postdeposition annealing (PDA) was performed at 400 °C. While the EOT was modest ( $<1 \mu\text{F}/\text{cm}^2$ ), plasma nitridation reduced the  $D_{it}$  by 10× compared to nonplasma treated samples to  $3.5 \times 10^{11} \text{ cm}^{-2} \text{ eV}^{-1}$  even with a nitride layer with 0.2 EOT; conversely, plasma oxidation increased the  $D_{it}$ . XPS studies showed that plasma oxidation increased GeO<sub>x</sub> but plasma nitridation transformed GeO<sub>x</sub> to

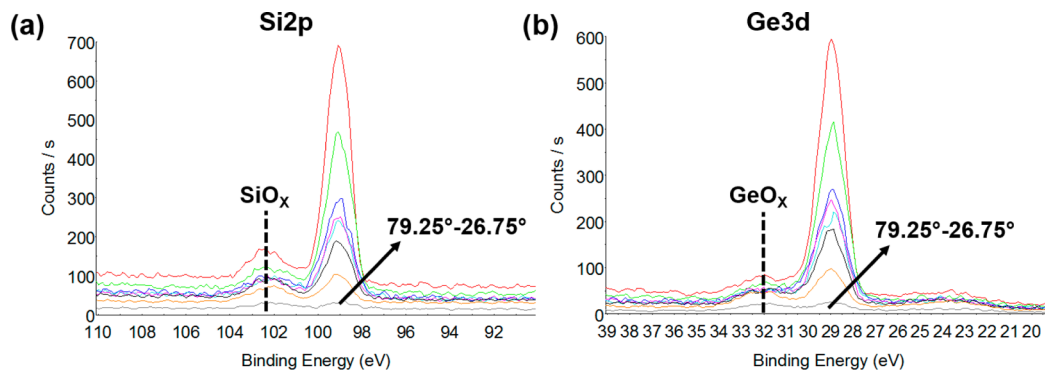


**Figure 7.** Angle resolved XPS spectra for Si 2p (a) and Ge 3d (b) showing the absence of  $\text{SiO}_2$  and  $\text{GeO}_2$  at the a- $\text{Al}_2\text{O}_3$ /SiGe interface.

GeON (possibly even  $\text{GeNx}$ ) consistent with a good interface forming between  $\text{Al}_2\text{O}_3$  and  $\text{Ge}(001)$  with only a monolayer of SiGeON at the interface.

## CONCLUSION

In summary, DFT-MD simulations show that a- $\text{Al}_2\text{O}_3$  stacked on SiGe can form high-quality abrupt unpinned interfaces with no midgap states. The internal bonds of a- $\text{Al}_2\text{O}_3$  are sufficiently strong to prevent Al intermixing and to allow just weak bonding to the SiGe surface. These weak interfacial bonds prevent formation of metallic-like Al–Si or Al–Ge states but leave dangling bonds. Although both Ge- and Si-terminated SiGe surfaces have dangling bonds, they can be tolerated in the absence of oxygen transfer because they are more filled and electrically passive. Even with oxygen transfer from the oxide to the SiGe surface dimers, the dangling bonds states are shallow states near the band edges and, therefore, barely change the band gap. The results show that oxide/semiconductor interfaces are very sensitive to small differences in bond strength and polarity even for isoelectronic surface atoms. C–V spectroscopy and angle-resolved X-ray photoelectron spectroscopy (AR-XPS) experiments on ALD a- $\text{Al}_2\text{O}_3$ /p-type SiGe(001) were consistent with the formation of interfaces with low interface trap density via direct bonding between SiGe and  $\text{Al}_2\text{O}_3$  without any  $\text{SiO}_2$  or  $\text{GeO}_2$  formation.

## ASSOCIATED CONTENT

### Supporting Information

The Supporting Information is available free of charge on the ACS Publications website at DOI: [10.1021/acsami.5b08727](https://doi.org/10.1021/acsami.5b08727).

Si–Al bond charge density. SiGe H-passivated reference system. ([PDF](#))

## AUTHOR INFORMATION

### Corresponding Author

\*E-mail: [echagarov@ucsd.edu](mailto:echagarov@ucsd.edu).

### Notes

The authors declare no competing financial interest.

## ACKNOWLEDGMENTS

The authors gratefully acknowledge support from SRC-GRC, Applied Materials, and NSF-DMR NSF DMR1207213.

## REFERENCES

- (1) Green, M.; Gusev, E.; Degraeve, R.; Garfunkel, E. Ultrathin (<4 nm)  $\text{SiO}_2$  and Si–O–N Gate Dielectric Layers for Silicon Micro-

electronics: Understanding the Processing, Structure, and Physical and Electrical Limits. *J. Appl. Phys.* **2001**, *90*, 2057–2121.

(2) Garfunkel, E.; Gusev, E.; Vul', A. *Fundamental Aspects of Ultrathin Dielectrics on Si-based Devices*, 1st ed.; Springer: Netherlands, 1998.

(3) Mott, N.; Rigo, S.; Rochet, F.; Stoneham, A. Oxidation of Silicon. *Philos. Mag. B* **1989**, *60*, 189–212.

(4) Buchanan, D. A. Scaling the Gate Dielectric: Materials, Integration and Reliability. *IBM J. Res. Dev.* **1999**, *43*, 245–264.

(5) Gusev, E. P.; Narayanan, V.; Frank, M. M. Advanced High-k Dielectric Stacks with Poly-Si and Metal Gates: Recent Progress and Current Challenges. *IBM J. Res. Dev.* **2006**, *50*, 387–410.

(6) Balk, P. Dielectrics for Field Effect Technology. *Adv. Mater.* **1995**, *7*, 703–710.

(7) Atalla, M. M.; Tannenbaum, E.; Scheibner, E. Stabilization of Silicon Surface by Thermally Grown Oxide. *Bell Syst. Tech. J.* **1959**, *38*, 749–783.

(8) Ligenza, J.; Spitzer, W. The Mechanisms for Silicon Oxidation in Steam and Oxygen. *J. Phys. Chem. Solids* **1960**, *14*, 131–136.

(9) Lo, S.; Buchanan, D.; Taur, Y.; Wang, W. Quantum-Mechanical Modeling of Electron Tunneling Current from Inversion Layer of Ultra-Thin-Oxide nMOSFET's. *IEEE Electron Device Lett.* **1997**, *18*, 209–211.

(10) Buchanan, D.; Lo, S. *Physics and Chemistry of  $\text{SiO}_2$  and the Si– $\text{SiO}_2$  Interface*; Book Series: Electrochemical Society Series; Electrochemical Society: Pennington, NJ, 1996; pp 319–322.

(11) Wilk, G. D.; Wallace, R. M.; Anthony, J. High-k Gate Dielectrics: Current Status and Materials Properties Considerations. *J. Appl. Phys.* **2001**, *89*, 5243–5275.

(12) Houssa, M. *High k Gate Dielectrics*, 1st ed; CRC Press: Boca Raton, FL, 2003.

(13) Gusev, E. P.; Buchanan, D. A.; Cartier, E.; Kumar, A.; DiMaria, D.; Guha, S.; Callegari, A.; Zafar, S.; Jamison, P. C.; Neumayer, D. A.; Copel, M.; Gribelyuk, M. A.; Okorn-Schmidt, H.; D'Emic, C.; Kozlowski, P.; Chan, K.; Bojarczuk, N.; Ragnarsson, L.-A.; Ronsheim, P.; Rim, K.; Fleming, R. J.; Mocuta, A.; Ajmera, A. Ultrathin High-K Gate Stacks for Advanced CMOS Devices. *IEDM Technol. Dig.* **2001**, 20.1.1–20.1.4.

(14) Welser, J.; Hoyt, J.; Takagi, S.-I.; Gibbons, J. Strain Dependence of the Performance Enhancement in Strained-Si n-MOSFETs. *IEDM Technol. Dig.* **1994**, 373–376.

(15) Welser, J.; Hoyt, J.; Gibbons, J. NMOS and PMOS Transistors Fabricated in Strained Silicon/Relaxed Silicon-Germanium Structures. *IEDM Technol. Dig.* **1989**, 1000–1002.

(16) Datta, S.; Brask, J.; Dewey, G.; Doczy, M.; Doyle, B.; Jin, B.; Kavalieros, J.; Metz, M.; Majumdar, A.; Radosavljevic, M. Advanced Si and SiGe Strained Channel NMOS and PMOS Transistors with High-k/Metal-Gate Stack. *Proceedings of the 2004 Bipolar/BICMOS Circuits and Technology Meeting Book Series: BCTM Proceedings* **2004**, 194–197.

(17) Robertson, J. High Dielectric Constant Gate Oxides for Metal Oxide Si Transistors. *Rep. Prog. Phys.* **2006**, *69*, 327–396.

(18) Gilmer, D.; Hegde, R.; Cotton, R.; Smith, J.; Dip, L.; Garcia, R.; Dhandapani, V.; Triyoso, D.; Roan, D.; Franke, A.; et al. Compatibility

- of Silicon Gates with Hafnium-Based Gate Dielectrics. *Microelectron. Eng.* **2003**, *69*, 138–144.
- (19) Kang, L.; Lee, B. H.; Qi, W.-J.; Jeon, Y.; Nieh, R.; Gopalan, S.; Onishi, K.; Lee, J. C. Electrical Characteristics of Highly Reliable Ultrathin Hafnium Oxide Gate Dielectric. *IEEE Electron Device Lett.* **2000**, *21*, 181–183.
- (20) Gusev, E.; Cabral, C., Jr.; Copel, M.; D'Emic, C.; Gribelyuk, M. Ultrathin  $\text{HfO}_2$  Films Grown on Silicon by Atomic Layer Deposition for Advanced Gate Dielectrics Applications. *Microelectron. Eng.* **2003**, *69*, 145–151.
- (21) Gusev, E.; Shang, H.; Copel, M.; Gribelyuk, M.; D'Emic, C.; Kozlowski, P.; Zabel, T. Microstructure and Thermal Stability of  $\text{HfO}_2$  Gate Dielectric Deposited on Ge(100). *Appl. Phys. Lett.* **2004**, *85*, 2334–2336.
- (22) Dimoulas, A.; Mavrou, G.; Vellianitis, G.; Evangelou, E.; Boukos, N.; Houssa, M.; Caymax, M.  $\text{HfO}_2$  High- $\kappa$  Gate Dielectrics on Ge (100) by Atomic Oxygen Beam Deposition. *Appl. Phys. Lett.* **2005**, *86*, 032908–032911.
- (23) Kuhn, K. J.; Murthy, A.; Kotlyar, R.; Kuhn, M. Past, Present and Future: SiGe and CMOS Transistor Scaling SiGe, Ge, and Related Compounds Plenary. *ECS Trans.* **2010**, *33*, 3–17.
- (24) Caymax, M.; Eneman, G.; Bellenger, F.; Merckling, C.; Delabie, A.; Wang, G.; Loo, R.; Simoen, E.; Mitard, J.; De Jaeger, B.; et al. Germanium for Advanced CMOS Anno 2009: a SWOT Analysis. *IEEE IEDM Book Series: International Electron Devices Meeting 2009*, 428–431.
- (25) Garrido, B.; Cuadras, A.; Bonafos, C.; Morante, J.; Fonseca, L.; Franz, M.; Pressel, K. Thermal Dry Oxidation of  $\text{Si}_{1-x-y}\text{Ge}_x\text{C}_y$  Strained Layers Grown on Silicon. *Microelectron. Eng.* **1999**, *48*, 207–210.
- (26) Frank, M. M.; Kim, S.; Brown, S. L.; Bruley, J.; Copel, M.; Hopstaken, M.; Chudzik, M.; Narayanan, V. Scaling the MOSFET Gate Dielectric: From High- $\kappa$  to Higher- $\kappa$ ? *Microelectron. Eng.* **2009**, *86*, 1603–1608.
- (27) Guha, S.; Gusev, E.; Copel, M.; Ragnarsson, L.-Å.; Buchanan, D. A. Compatibility Challenges for High-Kappa Materials Integration into CMOS Technology. *MRS Bull.* **2002**, *27*, 226–229.
- (28) Curreem, K.; Lee, P.; Wong, K.; Dai, J.; Zhou, M.; Wang, J.; Li, Q. Comparison of Interfacial and Electrical Characteristics of  $\text{HfO}_2$  and  $\text{HfAlO}$  High- $\kappa$  Dielectrics on Compressively Strained  $\text{Si}_{1-x}\text{Ge}_x$ . *Appl. Phys. Lett.* **2006**, *88*, 182905–182908.
- (29) Kamata, Y. High- $\kappa$ /Ge MOSFETs for Future Nanoelectronics. *Mater. Today* **2008**, *11*, 30–38.
- (30) Lu, N.; Bai, W.; Ramirez, A.; Mouli, C.; Ritenour, A.; Lee, M. L.; Antoniadis, D.; Kwong, D. L. Ge Diffusion in Ge Metal Oxide Semiconductor with Chemical Vapor Deposition  $\text{HfO}_2$  Dielectric. *Appl. Phys. Lett.* **2005**, *87*, 051922–051925.
- (31) Swaminathan, S.; Shandalov, M.; Oshima, Y.; McIntyre, P. C. Bilayer Metal Oxide Gate Insulators for Scaled Ge-Channel Metal-Oxide-Semiconductor Devices. *Appl. Phys. Lett.* **2010**, *96*, 082904–082907.
- (32) Wang, H.-B.; Ma, D.-Y.; Ma, F.; Xu, K.-W. Impact of Ultrathin  $\text{Al}_2\text{O}_3$  Interlayer on Thermal Stability and Leakage Current Properties of  $\text{TiO}_2/\text{Al}_2\text{O}_3$  Stacking Dielectrics. *J. Vac. Sci. Technol., B: Microelectron. Process. Phenom.* **2012**, *30*, 040601–040606.
- (33) Wu, D.; Lu, J.; Vainonen-Ahlgren, E.; Tois, E.; Tuominen, M.; Östling, M.; Zhang, S.-L. Structural and Electrical Characterization of  $\text{Al}_2\text{O}_3/\text{HfO}_2/\text{Al}_2\text{O}_3$  on Strained SiGe. *Solid-State Electron.* **2005**, *49*, 193–197.
- (34) Li, H.; Lin, L.; Robertson, J. Identifying a Suitable Passivation Route for Ge Interfaces. *Appl. Phys. Lett.* **2012**, *101*, 052903–052907.
- (35) Jernigan, G. G.; Thompson, P. E.; Silvestre, C. L. Quantitative Measurements of Ge Surface Segregation During SiGe Alloy Growth. *Surf. Sci.* **1997**, *380*, 417–426.
- (36) Godbey, D.; Ancona, M. Ge Profile from the Growth of SiGe Buried Layers by Molecular Beam Epitaxy. *Appl. Phys. Lett.* **1992**, *61*, 2217–2219.
- (37) Godbey, D.; Ancona, M. Concentration Dependence of Ge Segregation During the Growth of a SiGe Buried Layer. *J. Vac. Sci. Technol., B: Microelectron. Process. Phenom.* **1993**, *11*, 1392–1395.
- (38) Lin, D.-S.; Pan, S.-Y.; Wu, M.-W. Chlorine-Induced Si Surface Segregation on the Ge-Terminated Si/Ge(100) Surface from Core-Level Photoemission. *Phys. Rev. B: Condens. Matter Mater. Phys.* **2001**, *64*, 233302–233306.
- (39) Kaufman-Osborn, T.; Chagarov, E.; Park, S.-W.; Sahu, B.; Siddiqui, S.; Kummel, A. C. Atomic Imaging and Modeling of Passivation, Functionalization, and Atomic Layer Deposition Nucleation of the SiGe(001) Surface via  $\text{H}_2\text{O}_2(\text{g})$  and Trimethylaluminum Dosing. *Surf. Sci.* **2014**, *630*, 273–279.
- (40) Chagarov, E.; Kummel, A. Density Functional Theory Simulations of Amorphous High- $\kappa$  Oxides on a Compound Semiconductor Alloy:  $a\text{-Al}_2\text{O}_3/\text{InGaAs}(100)-(4 \times 2)$ ,  $a\text{-HfO}_2/\text{InGaAs}(100)-(4 \times 2)$ , and  $a\text{-ZrO}_2/\text{InGaAs}(100)-(4 \times 2)$ . *J. Chem. Phys.* **2011**, *135*, 244705–244722.
- (41) Chagarov, E.; Kummel, A. Molecular Dynamics Simulation Comparison of Atomic Scale Intermixing at the Amorphous  $\text{Al}_2\text{O}_3$ /Semiconductor Interface for  $a\text{-Al}_2\text{O}_3/\text{Ge}$ ,  $a\text{-Al}_2\text{O}_3/\text{InGaAs}$ , and  $a\text{-Al}_2\text{O}_3/\text{InAlAs}/\text{InGaAs}$ . *Surf. Sci.* **2009**, *603*, 3191–3200.
- (42) Chagarov, E.; Kummel, A. Ab Initio Molecular Dynamics Simulations of Properties of  $a\text{-Al}_2\text{O}_3$  /Vacuum and  $a\text{-ZrO}_2$  /Vacuum vs.  $a\text{-Al}_2\text{O}_3/\text{Ge}(100)(2 \times 1)$  and  $a\text{-ZrO}_2/\text{Ge}(100)(2 \times 1)$  Interfaces. *J. Chem. Phys.* **2009**, *130*, 124717–124731.
- (43) Kresse, G.; Furthmüller, J. Efficiency of Ab-initio Total Energy Calculations for Metals and Semiconductors Using a Plane-Wave Basis Set. *Comput. Mater. Sci.* **1996**, *6*, 15–50.
- (44) Kresse, G.; Furthmüller, J. Efficient Iterative Schemes for Ab Initio Total-Energy Calculations Using a Plane-Wave Basis Set. *Phys. Rev. B: Condens. Matter Mater. Phys.* **1996**, *54*, 11169–11186.
- (45) Perdew, J. P.; Burke, K.; Ernzerhof, M. Generalized Gradient Approximation Made Simple. *Phys. Rev. Lett.* **1996**, *77*, 3865–3868.
- (46) Perdew, J. P.; Burke, K.; Wang, Y. Erratum: Generalized Gradient Approximation for the Exchange-Correlation Hole of a Many-Electron System [Phys. Rev. B 54, 16 533 (1996)]. *Phys. Rev. B: Condens. Matter Mater. Phys.* **1998**, *57*, 14999–14999.
- (47) Heyd, J.; Scuseria, G. E.; Ernzerhof, M. Hybrid Functionals Based on a Screened Coulomb Potential. *J. Chem. Phys.* **2003**, *118*, 8207–8215.
- (48) Heyd, J.; Scuseria, G. E. Efficient Hybrid Density Functional Calculations in Solids: Assessment of the Heyd–Scuseria–Ernzerhof Screened Coulomb Hybrid Functional. *J. Chem. Phys.* **2004**, *121*, 1187–1192.
- (49) Heyd, J.; Scuseria, G. E.; Ernzerhof, M. Erratum: “Hybrid Functionals Based on a Screened Coulomb Potential” [J. Chem. Phys. 118, 8207 (2003)]. *J. Chem. Phys.* **2006**, *124*, 219906–219906.
- (50) Kruckau, A. V.; Vydrov, O. A.; Izmaylov, A. F.; Scuseria, G. E. Influence of the Exchange Screening Parameter on the Performance of Screened Hybrid Functionals. *J. Chem. Phys.* **2006**, *125*, 224106–224110.
- (51) Blöchl, P. E. Projector Augmented-Wave Method. *Phys. Rev. B: Condens. Matter Mater. Phys.* **1994**, *50*, 17953–17979.
- (52) Kresse, G.; Joubert, J. From Ultrasoft Pseudopotentials to the Projector Augmented-Wave Method. *Phys. Rev. B: Condens. Matter Mater. Phys.* **1999**, *59*, 1758–1775.
- (53) Tang, W.; Sanville, E.; Henkelman, G. A Grid-Based Bader Analysis Algorithm Without Lattice Bias. *J. Phys.: Condens. Matter* **2009**, *21*, 084204–084210.
- (54) Sanville, E.; Kenny, S. D.; Smith, R.; Henkelman, G. Improved Grid-Based Algorithm for Bader Charge Allocation. *J. Comput. Chem.* **2007**, *28*, 899–908.
- (55) Henkelman, G.; Arnaldsson, A.; Jónsson, H. A Fast and Robust Algorithm for Bader Decomposition of Charge Density. *Comput. Mater. Sci.* **2006**, *36*, 354–360.
- (56) Kaufman-Osborn, T.; Chagarov, E.; Park, S.-W.; Sahu, B.; Siddiqui, S.; Kummel, A. C. Atomic Imaging and Modeling of Passivation, Functionalization, and Atomic Layer Deposition Nucleation of the SiGe(001) Surface via  $\text{H}_2\text{O}_2(\text{g})$  and Trimethylaluminum Dosing. *Surf. Sci.* **2014**, *630*, 273–279.
- (57) Oshima, Y.; Sun, Y.; Kuzum, D.; Sugawara, T.; Saraswat, K. C.; Pianetta, P.; McIntyre, P. C. Chemical Bonding, Interfaces, and

Defects in Hafnium Oxide/Germanium Oxynitride Gate Stacks on Ge(100) Dielectric Science and Materials. *J. Electrochem. Soc.* **2008**, *155*, G304–G309.

(58) Zhang, R.; Iwasaki, T.; Taoka, N.; Takenaka, M.; Takagi, S. High Mobility Ge pMOSFETs with ~1nm Thin EOT Using  $\text{Al}_2\text{O}_3/\text{GeOx}/\text{Ge}$  Gate Stacks Fabricated by Plasma Post Oxidation. *2011 IEEE Symp. VLSI Technol., Dig. Technol. Pap.* **2011**, 56–57.

(59) Yu, T.; Jin, C. G.; Yang, Y.; Zhuge, L. J.; Wu, X. M.; Wu, Z. F. Effect of  $\text{NH}_3$  Plasma Treatment on the Interfacial Property between Ultrathin  $\text{HfO}_2$  and Strained  $\text{Si}_{0.65}\text{Ge}_{0.35}$  Substrate. *J. Appl. Phys.* **2013**, *113*, 044105–044106.

(60) Li, C.-C.; Chang-Liao, K.-S.; Fu, C.-H.; Tzeng, T.-H.; Lu, C.-C.; Hong, H.-Z.; Chen, T.-C.; Wang, T.-K.; Tsai, W.-F.; Ai, C.-F. Electrical Characteristics of SiGe pMOSFET Devices with Tantalum or Titanium Oxide Higher-k Dielectric Stack. *Solid-State Electron.* **2012**, *78*, 17–21.

(61) Frank, M. M.; Cartier, E. A.; Ando, T.; Bedell, S. W.; Bruley, J.; Zhu, Y.; Narayanan, V. Aggressive SiGe Channel Gate Stack Scaling by Remote Oxygen Scavenging: Gate-First pFET Performance and Reliability. *ECS Trans.* **2013**, *50*, 275–280.

(62) Han, J.-H.; Zhang, R.; Osada, T.; Hata, M.; Takenaka, M.; Takagi, S. Impact of Plasma Post-Nitridation on  $\text{HfO}_2/\text{Al}_2\text{O}_3/\text{SiGe}$  Gate Stacks Toward EOT Scaling. *Microelectron. Eng.* **2013**, *109*, 266–269.

(63) Han, J.; Zhang, R.; Osada, T.; Hata, M.; Takenaka, M.; Takagi, S. Reduction in Interface Trap Density of  $\text{Al}_2\text{O}_3/\text{SiGe}$  Gate Stack by Electron Cyclotron Resonance Plasma Post-nitridation. *Appl. Phys. Express* **2013**, *6*, 051302–051303.